2013 IEEE/RSJ International Conference on
Intelligent Robots and Systems (IROS)
November 3-7, 2013. Tokyo, Japan

Task-Specific Evaluation of Kinematic Designs for Instruments in Minimally Invasive Robotic Surgery

Bastian Deutschmann, Rainer Konietschke and Alin Albu-Schäffer

***Abstract*— In minimally invasive robotic surgery, slender instruments are used that provide additional degrees of freedom inside the human body. Kinematic limitations due to the instrument could endanger the secure execution of a surgical task. Numerous design alternatives are proposed in literature whereas few work is done that evaluates the performance of these instruments objectively. This paper presents a new method to evaluate alternative designs of instrument kinematics with respect to their ability to perform surgical tasks. Two specific criteria are set up accounting for the limited space during a minimally invasive intervention as well as for the ability to execute the desired task. The evaluation is based on task specific reference trajectories which are recorded in one orientation. During robotic surgery, arbitrary orientations of this area can occur. The method is able to handle this by rotating the acquired reference trajectories within software. The presented method is independent from the setup, i.e. the relative position and orientation of the area of interest with respect to the trocar location. Four different examples demonstrate the application of the method to show its usefulness.**

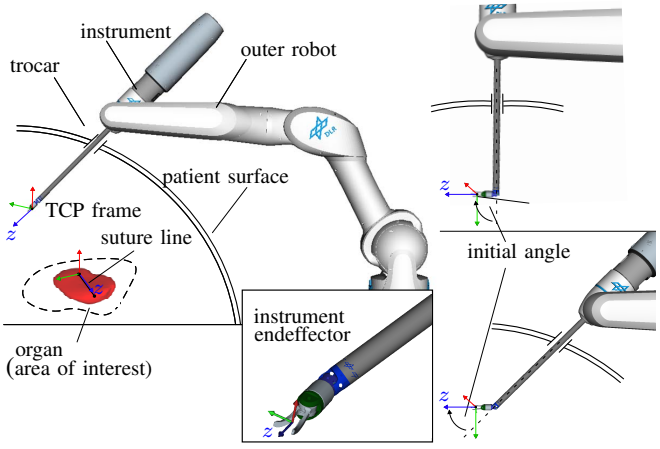

Fig. 1. Left: Common setup in minimally invasive robotic surgery. An outer robot carries an instrument (adapted from [25]). Right: Different innitial angles for a steep (top) and a gentle approach of the instrument (bottom)

I. INTRODUCTION

In robotic telesurgery for minimally invasive interventions, a surgeon on an input console (master) telemanipulates a robotic system (slave) at the patient side. The common setup is an outer robot that carries an instrument equipped with a slender shaft and specially designed endeffectors inside the patient, see Fig. 1. The entry port to the patient (trocar) which is necessary to insert the shaft and endeffector, blocks two degrees of freedom (DoF) of the robotic system and thus resembles a kinematic constraint. In order to compensate for this trocar constraint, the instrument inside the patient body is equipped with additional DoFs at the endeffector.
The desire of surgeons is a manipulation without limitations in situ and a secure execution of typical tasks. In minimally invasive interventions, these tasks are e.g. clamping and displacing tissue, dissection of organs or vessels as well as placing a suture and surgical knot tying. The inability of the slave robot to reach a certain pose at the area of interest is a severe restriction of performance. Commonly, the outside robot is responsible for the position whereas the instrument is responsible for the orientation of the tool center point (TCP). Thus, limitations in positioning and orientating can be addressed to the robot and instrument respectively.

Numerous designs of instruments for minimally invasive surgery can be found in relevant literature, e.g. [1]–[8]. An evaluation of these designs based on quantitative measures that display the influence of design specific parameters, e.g. the joint sequence, the joint range or the link length, help to improve the performance of given designs with respect to (w.r.t.) a demand or task. Different alternatives for instruments can be evaluated prior to building prototypes and thus reduce costs and save time. A criterion that assesses the performance of different instrument designs would also be beneficial during the planning phase of a minimally invasive robotic surgery.

This paper presents a new method to evaluate alternative configurations of instrument kinematics w.r.t. their ability to perform surgical tasks. Two criteria are established that account for 1) the confined space during a minimally invasive intervention and for 2) the ability to execute the desired task. Therefore an abstract task description is developed that considers a surgical task as a trajectory related to a specified position and orientation within the area of interest, for example the pose of the suture line (Fig. 1). In contrast to proposed methods from the literature, one advantage of the presented method is its independence from the setup, i.e. the relative position and orientation of the area of interest w.r.t. the trocar location.

The paper is structured by four sections. In Sec. II, preliminary terms and definitions are given and a review of instrument designs and evaluation methods from literature is presented. Subsequently in Sec. III, the proposed method will be presented and Sec. IV assesses the proposed method on the basis of four examples. Sec. V revises benefits and limitations of the method and gives perspectives for future developments.

The authors are with the German Aerospace Center (DLR), Institute of Robotics and Mechatronics, 82234 Oberpfaffenhofen, Germany
bastian.deutschmann at dlr.de

II. PRELIMINARIES

This section classifies design alternatives for minimally invasive instruments. A terminology to structure the evaluation methods is given and a review of evaluation methods in literature is presented.

A. Classification of Instrument Kinematics

To reach an arbitrary Cartisian pose within the patient, 6DoF are necessary. Considering the outer robot maintaining 3 translational DoF and 1 additional rotational DoF within the patient, the instruments for minimally invasive robotic surgery have to provide at least 2 independent rotational DoFs. Those DoF are commonly implemented as pitch (p) and yaw (y) joints with a preferable large range of motion [1]–[8]. Occasional, the desired range of motion can not be provided by a single joint due to mechanical limitations. In this case, multiple joints can be attached serially to each other in order to enlarge the motion range. Although more joints than degrees of freedom are considered, redundancy is not examined here. This is done by introducing the linear relationship

$$i_{kin} = \frac{q_{p,i}}{q_{p,j}} \tag{1}$$

that describes the magnitudal ratio of two adjacent joints, e.g. $q_{p,i}$ and $q_{p,j}$ with the same axis of rotation, see Fig. 2. Thus, the description of an instrument design with one pitch DoF (q_p) and one yaw DoF (q_y) is sufficient.

Design alternatives of minimally invasive instruments range from continuous (cont.) designs with flexible stems to discrete joints (disc.), serially attached to each other. These alternatives are classified according to the DH-notation [15], where two adjacent joints are connected by a link of a certain length. For the further proceeding of this paper, design parameters that influence the capabilities of the instrument are considered to be the number of joint axes n_j, the number of links n_l as well as the geometric parameters link length l_{link}, joint limits q_{lim} and ratio i_{kin}. An example for this classification is given in Fig. 2. Two universal joints (u), $n_j = 4$, are serially attached to each other by two links $n_l = 2$ links respectively. A universal joint therefore has two intersecting pitch (p) and yaw (y) axis. Tab. I comprises several kinematic designs from literature classified in the described manner.

TABLE I

PARAMETERS FOR THE CLASSIFICATION OF JOINT DESIGNS FOR MINIMALLY INVASIVE ROBOTIC SURGERY

Ref. (type)	n_l	n_j	$l_{link}[mm]$	$q_{lim}\,[^\circ]$	i_{kin}
[1] (disc.)	1	2 (u)	10	±40	-
[2] (disc.)	2	4 (u)	2.5	±45	1
[3] (disc.)	4	8 (u)	5	±25	1
[4] (disc.)	2	2 (py)	5	±90	1
[5] (disc.)	4	4 (pyyp)	–	±45	1
[6] (disc.)	4	4 (pyyp)	–	±45	1
[7] (cont.)	1	2	28	±40	-
[8] (disc.)	7	1 (p)	–	±30	0.8-1.5

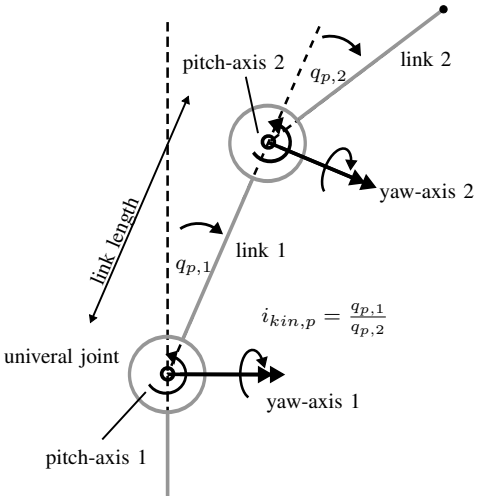

Fig. 2. Scheme of the design proposed from [2] according to the presented classification rotated around the pitch axes.

B. Terminology

Setup: The term *setup* comprehends the relative position of the trocar w.r.t. the position and orientation of the area of interest, e.g. the surface of an organ. This setup determines the initial angle (pitch and yaw) to approach the desired area of interest (desired TCP frame) and therefore has a strong influence on whether the instrument is able to perform a task. An example is depicted in Fig. 1 on the right for a steep (top) and gentle (bottom) approach.

Evaluation Methods: Methods to evaluate the kinematic configuration of manipulators (in general) apply criteria for performance evaluation while executing a desired task. According to literature, a *task* can range from a single pose to a discrete set of poses, which the TCP of the manipulator has to reach. Or a specific trajectory i.e. a temporal sequence of discrete poses related to the field of application (e.g. surgery). A *criterion* can be defined as a metric to evaluate the quality of performance of a mechanism. Since the defined task and the defined criteria are the most relevant part of every evaluation, subsequent methods for evaluation are organized in terms of *criterion* and *task*.

C. State of the Art in Evaluation Methods

General criteria to evaluate the kinematic design examine the total range of orientation [9], [10] or the distance towards the joint limits [19] without specifying a task. With such criteria, quantitative comparisons can be made. However, for manipulators in minimally invasive robotic surgery, these criteria directly reflect the joint limits of the instrument and are strongly dependent on the setup.

Other general criteria are based on the manipulators Jacobian Matrix $\boldsymbol{J}$ like the *manipulability* w in [17] or the condition number $c(\boldsymbol{J})$ in [19], describing the ease of positioning and orientating at a certain set of joint angles $\boldsymbol{q}$. These measures degrade close to a singularity, without accounting for the absolute distance to it. A further limitation is that $\boldsymbol{J}$ is dependent on the unit of $\boldsymbol{q}$ and $\dot{\boldsymbol{q}}$.

The suggested methods from [16] and [13] apply the mentioned criteria, manipulability measure w and condition number $c(\boldsymbol{J})$, to evaluate alternatives for minimally invasive instruments and a single port instruments respectively. The task in [13] is a modeled needle insertion trajectory (single rotation along needle centre) while sampling different positions and initial orientations of the needle in the workspace. The method is able to evaluate the superiority of one design w.r.t. the trocar pose. Cavusoglu [16] utilizes a knot tying trajectory recorded from expert surgeons in an open surgery test bed as a task. He evaluates two alternative instruments qualitatively and suggests a preferred design for each relevant setup positions.
Ankur [12] also performed ideal needle insertions as a task. The criterion is the absolute (translational) movement of the base joints that are not part of the instrument. He is able to justify his snake like instrument with this method, whereas the setup dependency is not examined.
Faraz [14] utilizes the *dexterous workspace* criterion while sampling the circular workspace around the trocar in one plane. He considers designs of minimally invasive instruments to be dexterous if a remaining motion range of at least 60° is left at each sampled point. The criterion indicates the percentage of these dexterous points in the workspace. Limitations of this approach are the plain examination and that the bending requirement is mainly accounting for joint ranges whereas other design parameters play a secondary role.
The method suggested in [18] evaluates different kinematic designs of handheld instruments while expert surgeons are performing suturing tasks in a simulated test environment. Their criterion is the *task completion time*, which is a relevant criteria evaluating surgeons skills, but does not reflect kinematic properties and its geometric origin at all.
Konietschke [11] utilizes several criteria like a predefined accuracy or the mean distance to the joint limits to find the optimal link length of a redundant robot. The task is to reach discrete points in a predefined volume with an additional variation of the TCP orientation. The method accounts for the translational limitations of the medical robot and is therefore not applicable to evaluate instrument designs.

III. METHOD

This section introduces the set of necessary coordinate systems and the acquisition of the task specific reference trajectory including its further processing to express the reference trajectories in arbitrary orientations. The criteria that are used for the evaluation are introduced. Furthermore, the applied forward and inverse kinematics algorithm is presented and the six necessary steps to implement the method.

A. Assigned coordinate frames

A coordinate frame is considered to be a homogeneous transformation $\boldsymbol{T} \in \mathbb{R}^{4\times4}$ [15] with position $\boldsymbol{t} \in \mathbb{R}^3$ and orientation $\boldsymbol{R} \in \mathbb{R}^{3\times3}$ w.r.t. a reference frame.
The global reference frame for the evaluation method is attached to the trocar $\boldsymbol{T}_{Tr}$. A second frame is attached to the area of interest (see Fig. 1), denoted as the suture line (SL) in the following, where a task needs to be fulfilled. This frame has a certain distance ${}^{Tr}\boldsymbol{t}_{SL}$ and initial orientation ${}^{Tr}\boldsymbol{R}_{SL,init}$ towards the trocar frame,

$$ {}^{Tr}\boldsymbol{T}_{SL} = \begin{bmatrix} {}^{Tr}\boldsymbol{R}_{SL,init} & {}^{Tr}\boldsymbol{t}_{SL} \\ \boldsymbol{0} & 1 \end{bmatrix}. \tag{2} $$

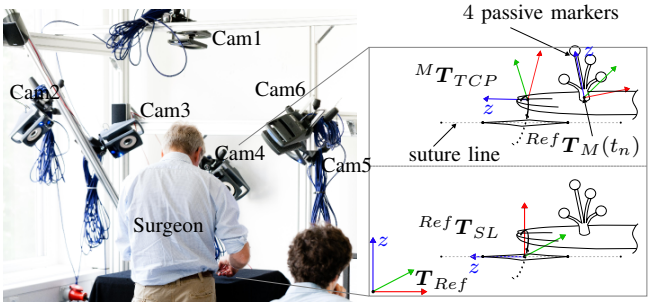

Fig. 3. Left: Setup of the six Vicon cameras (cam1 ... cam6) with expert surgeon performing knot tying. Right: Assigned coordinates frame necessary for the calibration

B. Task

The program "Fundamentals of Laparoscopic Surgery" (FLS) considers *tying a knot* as one of seven most fundamental skills in laparoscopic surgery [21]. Therefore, this basic [23] and vital component of any surgeons skill set [22] must be performed reliably especially in robotic surgery [20].
We recorded knot tying trajectories in an open surgery test bed where five expert surgeons and one trainee were asked to perform standard sized surgical knots (standard double schiffer knot with standard sized suture material, 3.0 Monocryl leash, violet, 22 mm, $1/2c$, visiblack needle). A needle holder and a forceps were used as right handed and left handed instrument. The motion of the needle holder was captured with a Vicon MX motion tracking system (see Fig. 3, left). Four passive markers, rigidly connected to each other, were fixed to the surgical tool. Six near-infrared cameras reconstructed the tool's pose ${}^{Ref}\boldsymbol{T}_{M}(t_n)$ at each time stamp t_n with a sampling rate of 100 Hz. The tracking error of one marker can be considered as below $0.1\ mm$. The frames are given relative to a reference frame $\boldsymbol{T}_{Ref}$ that was set up during the Vicon calibration phase.
To calibrate the TCP of the needleholder to the captured marker M, a constant calibration frame ${}^{M}\boldsymbol{T}_{TCP}$ is assigned by a second marker-target (see Fig. 3, right top) which is attached to the location of needleholder's TCP,

$$ {}^{Ref}\boldsymbol{T}_{TCP}(t_n) = {}^{Ref}\boldsymbol{T}_{M}(t_n) \cdot {}^{M}\boldsymbol{T}_{TCP}. \tag{3} $$

The z-axis of this second target is aligned with the needleholder's long axis. A second reference frame ${}^{Ref}\boldsymbol{T}_{SL}$ is attached to the suture line (see Fig. 3, right bottom) which originates at the insertion point and matches the suture line direction by its z- axis. This frame relates the TCP frame trajectory (Eq.3) to the suture line

$$ {}^{SL}\boldsymbol{T}_{TCP}(t_n) = {}^{Ref}\boldsymbol{T}_{SL}^{-1} \cdot {}^{Ref}\boldsymbol{T}_{M}(t_n) \cdot {}^{M}\boldsymbol{T}_{TCP}. \tag{4} $$

The duration of reference trajectories from expert surgeons ranges from $T = 25.6/33.2$ s leading to the total number N_T of frames per trajectory,

$$N_T = \frac{25.6s/33.2s}{100Hz} = 2560/3320. \quad (5)$$

An instrument has to enable a trajectory in a diversity of orientations in a minimally invasive intervention. To account for this diversity, the initial orientation of the suture line ${}^{Tr}\boldsymbol{R}_{SL,init}$ is varied in discrete steps along all axes. The knot-trajectory ${}^{SL}\boldsymbol{T}_{TCP}(t_n)$ then is performed at each initial orientation. As the method proposes an evaluation on the base of all possible orientations, it is independent from the trocar position.

The set $\boldsymbol{W}_{SL}$ of all possibel suture line orientations can be generated in multiple ways. One way is described in the following. At first, the initial orientation ${}^{Tr}\boldsymbol{R}_{SL,init}$ is rotated about the y_{init}-axis with β_i and about the z_{init}-axis with α_k, see Fig. 4. Additionally the orientation is rotated about the instantanous z-axis with γ_j to account for a circular variation of the insertion point. The introduced angles are

$$\beta_i = i \cdot S_\beta, \quad i \in [0 \dots N_\beta], \quad N_\beta = \frac{\pi}{S_\beta} - 1 \quad (6)$$

$$\alpha_k = k \cdot S_\alpha, \quad k \in [1 \dots N_\alpha], \quad N_\alpha = \frac{2\pi}{S_\alpha} - 1 \quad (7)$$

$$\gamma_j = j \cdot S_\gamma, \quad j \in [1 \dots N_\gamma], \quad N_\gamma = \frac{2\pi}{S_\gamma} - 1. \quad (8)$$

with $\{S_\beta, S_\gamma, S_\alpha\} \in \mathbb{R}$ embodying discrete angular steps. The described total rotation of the suture line orientation ${}^{Tr}\boldsymbol{R}_{SL}$ is expressed as

$${}^{Tr}\boldsymbol{R}_{SL,i,j,k} = {}^{Tr}\boldsymbol{R}_{SL,init} \cdot \boldsymbol{R}_y(\beta_i) \cdot \boldsymbol{R}_z(\gamma_j) \cdot \boldsymbol{R}_{z'}(\alpha_k). \quad (9)$$

resulting in a total number of

$$N = N_\beta \cdot N_\gamma \cdot N_\alpha \quad (10)$$

orientations. The task set $\boldsymbol{W}_{SL}$ considered in this work comprehends all created suture line orientations,

$$\boldsymbol{W}_{SL} = \{{}^{Tr}\boldsymbol{T}_{SL,l} \in \mathbb{R}^{4\times4} | {}^{Tr}\boldsymbol{T}_{SL} = {}^{Tr}\boldsymbol{T}_{SL,l}\} \subset \mathbb{R}^4, \quad \forall l \in \{1 \dots N\} \quad (11)$$

with

$${}^{Tr}\boldsymbol{T}_{SL,l} = \begin{bmatrix} {}^{Tr}\boldsymbol{R}_{SL,l} & {}^{Tr}\boldsymbol{t}_{SL} \\ \boldsymbol{0} & 1 \end{bmatrix}. \quad (12)$$

The overall task covers the execution of a knot tying trajectory starting from each suture line orientation defined in $\boldsymbol{W}_{SL}$ (Eq.11). Therefore, N (Eq.10) desired trajectories for a TCP motion are given,

$${}^{Tr}\boldsymbol{T}_{TCP,l}(t_n) = {}^{Tr}\boldsymbol{T}_{SL,l} \cdot {}^{SL}\boldsymbol{T}_{TCP}(t_n), \quad \forall l \in \{1 \dots N\} \quad . \quad (13)$$

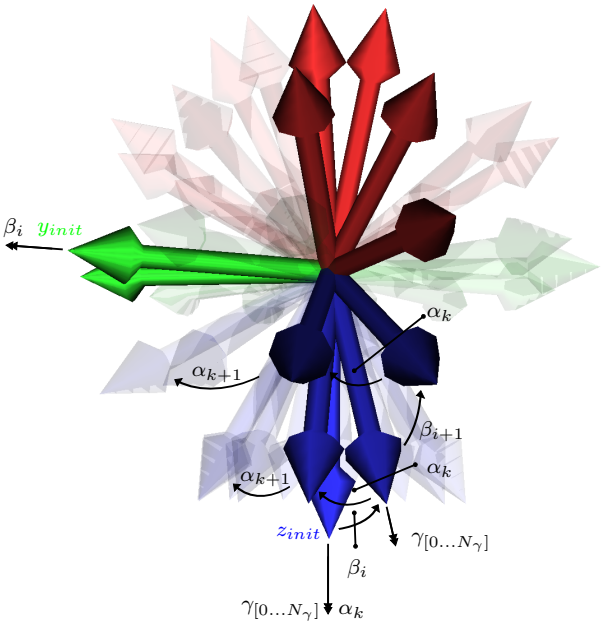

Fig. 4. Variation of suture line orientation ${}^{Tr}\boldsymbol{R}_{SL,init}$ (suture line $\rightarrow$ z-axis). The rotation axis y_{init} for β_i and z_{init} for α_k are constant while generating the set of orientations $\boldsymbol{W}_{SL}$.

C. Criteria

The applied criteria are denoted as the *Success Rate* SUR and the *Shaft Distance* d_{IB} which will be explained in the following.

Success Rate: As mentioned in the previous paragraph, an instrument needs to execute crucial tasks, like knot tying, thoroughly. To account for this capability, the Success Rate is introduced. N trajectories (Eq.10) are utilized during the task execution. The number of feasible task trajectories $N_c <= N$, i.e. trajectories that are performed without reaching a joint limit, is

$$N_c = \sum_{l=1}^{N} floor \left[\frac{1}{N_T} \sum_{n=1}^{N_T} sign\left(\boldsymbol{q}_{lim} - \boldsymbol{q}_{instr,t_n,l}\right) \right]. \quad (14)$$

$\boldsymbol{q}_{lim}$ are predefined joint limits and $\boldsymbol{q}_{instr,t_n,l}$ are the joint angles of the instrument at time stamp t_n of the l^{th} trajectory. The ratio of N_c and N is denoted as the Success Rate

$$SUR = \frac{N_c}{N} \cdot 100\,[\%]. \quad (15)$$

A Success Ratio of $SUR = 100\%$ indicates that the instrument is able to perform all sampled trajectories completely. High values for SUR indicate therefore preferable instrument designs. The $floor$-function in equation (Eq. 14) ensures that only successfully performed trajectories without reaching a joint limit at every discrete point are taken into account to determine N_c.

Shaft Distance: Space is limited in minimally invasive interventions and collisions of the instrument with inner structures of the patient have to be avoided. In particular, since the part of the instrument seen in the endoscope picture is rather

small, collisions of the instrument part not seen in the endoscope picture are a severe safety threat. The Shaft Distance criterion is introduced to consider the amount of radial space that is captured by an instrument. If an instrument rotates its TCP without translation, the end of the slender shaft, called instrument base ${}^{Tr}\boldsymbol{T}_{IB}$, has the largest radial distance (in the yz-plane) towards the trocar $\boldsymbol{T}_{Tr}$, see Fig. 5. The distance measure d_{IB} can therefore be calculated as

$$d_{IB} = \sqrt{y_{IB}^2 + z_{IB}^2}, \tag{16}$$

whereas y_{IB} and z_{IB} are the y- and z- coordinates of the IB-frame w.r.t. the trocar frame. The Shaft Distance criterion is calculated for all feasible tasks N_c (Eq.14) whereas the mean value and the standard deviation are considered for evaluation of the instrument. Small values for d_{IB} (Eq.16) indicates less radial space and therefore preferable instrument designs.

D. Forward and Inverse Kinematics

Within the paper, the outer robot and the inner instrument (Fig. 1) are approximated as one kinematic structure with 6DoF, see Fig. 5. The robot is approximated as a universal joint (q_1, q_2) and a prismatic joint (q_3) attached to the trocar to position the instrument inside the patient. Joint variables are $\boldsymbol{q}_{Tr} = [q_1, q_2, d_3]^T$ respectively. The instrument is attached to these trocar joints with its shaft and possesses three additional joints. The joints of the instrument $\boldsymbol{q}_{Inst} = [q_r, q_p, q_y]^T$ consist of a roll joint[1] along the shaft-axis q_r as well as a pitch q_p and a yaw joint q_y. The forward kinematics

TABLE II

DH-Parameters to calculate forward and inverse kinematics, exemplary shown for configuration [3]

Frame	a_{i-1}	α_{i-1}	d_i	θ_i
${}^{Tr}\boldsymbol{T}_1(q_1)$	0	0	0	0
${}^{1}\boldsymbol{T}_2(q_2)$	0	$-\frac{pi}{2}$	0	$-\frac{pi}{2}$
${}^{2}\boldsymbol{T}_3(d_3)$	0	$-\frac{pi}{2}$	d_{SL}	$-\frac{pi}{2}$
${}^{3}\boldsymbol{T}_r(q_r)$	0	0	0	$-\frac{pi}{2}$
${}^{r}\boldsymbol{T}_p(q_p, i_{kin})$	0	$-\frac{pi}{2}$	0	$-\frac{pi}{2}$
${}^{p}\boldsymbol{T}_y(q_y, i_{kin})$	0	$-\frac{pi}{2}$	0	0
${}^{y}\boldsymbol{T}_p(q_p, i_{kin})$	a_{shaft}	$\frac{pi}{2}$	0	0
${}^{p}\boldsymbol{T}_y(q_y, i_{kin})$	0	$\frac{pi}{2}$	0	0
${}^{y}\boldsymbol{T}_p(q_p, i_{kin})$	a_{shaft}	$\frac{pi}{2}$	0	0
${}^{p}\boldsymbol{T}_y(q_y, i_{kin})$	0	$\frac{pi}{2}$	0	0
${}^{y}\boldsymbol{T}_p(q_p, i_{kin})$	a_{shaft}	$\frac{pi}{2}$	0	0
${}^{p}\boldsymbol{T}_y(q_y, i_{kin})$	0	$\frac{pi}{2}$	0	0

is computed according to the DH-notation [15] and the introduced linear transmission ratio i_{kin} (Eq.1), yielding a homogeneous transformation

$$\begin{aligned} {}^{Tr}\boldsymbol{T}_{TCP}(\boldsymbol{q}) &= {}^{Tr}\boldsymbol{T}_1(q_1) \cdot {}^{1}\boldsymbol{T}_2(q_2) \cdot {}^{2}\boldsymbol{T}_3(q_3) \cdot \ldots \\ \ldots \cdot {}^{3}\boldsymbol{T}_r(q_r) &\cdot {}^{r}\boldsymbol{T}_p(q_p, i_{kin}) {}^{p}\boldsymbol{T}_y(q_y, i_{kin}) \cdot {}^{y}\boldsymbol{T}_{TCP} \end{aligned} \tag{17}$$

[1]The roll joint is sometimes part of the outer robot, depending on the system in focus. Since it mainly affects the orientation, it is counted among the instrument joints

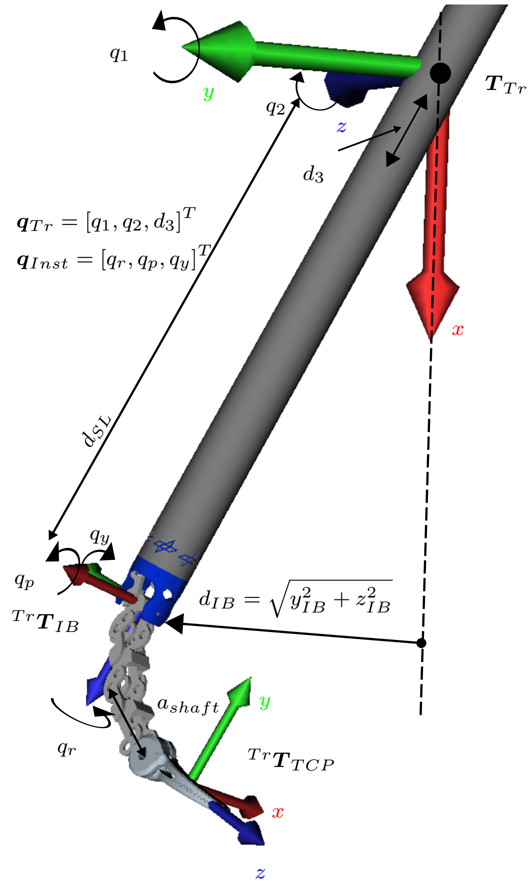

Fig. 5. Joint configuration (exemplary shown on a 4 link universal Joint ($4LU$) configuration), assigned frames and illustration of the Shaft Distance. 3D-CAD-Files from [1] (shaft) and [24] (Instrument)

that relates the joint angles

$$\boldsymbol{q} = [\boldsymbol{q}_{Tr}, \boldsymbol{q}_{Inst}]^T \tag{18}$$

to a TCP position and orientation w.r.t. the trocar frame $\boldsymbol{T}_{Tr}$. The respective DH-parameters are presented in Tab. II for an instrument with 4 links and a universal joint configuration, see [3]. The assigned constant transformation ${}^{y}\boldsymbol{T}_{TCP}$ in (Eq.17) is a rotation of 90° about the $y-$axis and a translation of a_{TCP} along the x-axis. To calculate the corresponding joint angles $\boldsymbol{q}$ to a desired TCP frame ${}^{Tr}\boldsymbol{T}_{TCP,l}(t_n)$, an inverse kinematic algorithm is implemented based on the inverse Jacobian Matrix and an iterative Newton-Raphson method [15]. The Jacobian matrix is calculated from the homogeneous transformations of each joint using the method described in [15]. Limitations of the trocar joints $\boldsymbol{q}_{Tr}$ are not considered since they describe translation boundaries due to the capabilities of the outer robot which should not affect the evaluation. To describe the limitations of each instrument respectively, joint limits of the instrument have to be predefined,

$$\boldsymbol{q}_{lim,Inst} = [q_{lim,r}, q_{lim,p}, q_{lim,y}]^T \tag{19}$$

E. Implementation

To evaluate different instruments with the presented method, a sequence of steps are necessary:

1) Instruments that are evaluated need to be selected → DH-Parameters of each instrument are derived yielding the homogeneous transformations for the forward and inverse kinematics (Eq.17)
2) Joint limits (Eq.19) are assigned. Based on these limits, a task is considered to be successfully executed or not later on
3) The discrete angular steps S_α, S_β and S_γ (Eq.8) are assigned that describe the density of the evaluated suture line orientations and the distance ${}^{Tr}\boldsymbol{t}_{SL}$ of the SL frame (Eq.2) to the trocar frame is determined → the set $\boldsymbol{W}_{SL}$ is generated
4) Execution of the inverse kinematics algorithm → set of joint angles $\boldsymbol{q}_{l,n}$ at each time stamp t_n and l initial orientation ($\boldsymbol{W}_{Sl}$, (Eq.11))
5) Determine the number of successfully performed trajectories by applying equation (Eq.14) and (Eq.15)
6) Calculation of the mean distance d_{IB} (Eq.16) and its standard deviation for the subset of successfully performed trajectories.

After a successive execution of the presented steps an instrument can be evaluated according to the criteria SUR and the mean d_{IB}.

IV. Examples

This section gives four examples to point out the usefulness of the proposed method. The results in all four cases are presented for one specified distance ${}^{Tr}\boldsymbol{t}_{SL} = [150, 0, 0]^T$ mm towards the trocar location. The angular steps S_β, S_γ and S_α are set to 30° (Eq.8) leading to a total number of $N = 726$ (Eq.10) suture line orientations. The utilized knot tying trajectory (individual knot of one surgeon) from the tracking experiment lasts $T = 27.3$ s yielding $N_T = 2730$ poses per trajectory. The limit of the roll joint is considered to be $q_{lim,r} = \pm 180°$ for all examples.

Variations in distance towards the trocar frame, $x_{SL,init}$, influence the results of the evaluation method. To examine the influence of a distance variation, an instrument with a 4 link design with 4 universal joints, a link length of $l_{link} = 5$ mm and a linear transmission ratio of $i_{kin} = 1.0$ ($4LU_{l5,i1}$) and joint ranges of about $q_{lim,py} = \pm 22.5°$ is examined w.r.t. different trocar distances, see Tab. III. Considering a variation of the distance to the trocar within 100 mm a slight influence on the criteria SUR and d_{IB} of 2.5% and 0.5 mm can be stated respectively.

The benchmarked trajectory for the present method is a knot trajectory from one subject (surgeon or trainee). It is not a unified trajectory of several recorded sutures and also no intersection is done between trajectories of different surgeons. Tab. IV displays the influence of trajectories recorded from different surgeons on the criteria Success Rate SUR and Shaft Distance d_{IB}. Eight trajectories per subject are evaluated. The applied instrument is again a $4LU_{l5,i1}$. Comparing each subject indiviually, the standard deviation values of both criteria display that the influence of different trajectories can not be neglected.

TABLE III
Influence of different trocar distances on the criteria SUR and mean Shaft Distance d_{IB}

$x_{SL,init}\,[mm]$	$q_{lim,py}\,[°]$	$SUR\,[\%]$	$d_{IB} \pm std\,[mm]$
70	±22.5	28.9	7.9 ± 2.4
100	±22.5	30.1	8.1 ± 2.5
120	±22.5	30.5	8.2 ± 2.5
150	±22.5	31.7	8.3 ± 2.6
170	±22.5	31.5	8.4 ± 2.6

TABLE IV
Trajectories from different subjects (Surgeons + Trainee) and their influence on the evaluation method

Subject	$mean(SUR) \pm std\,[\%]$	$d_{IB} \pm std\,[mm]$
Trainee	31.9 ± 0.7	8.5 ± 2.6
Surgeon 1	23.2 ± 5.7	8.2 ± 2.2
Surgeon 2	16.6 ± 4.4	8.8 ± 1.5
Surgeon 3	22.0 ± 1.2	7.7 ± 2.0
Surgeon 4	30.1 ± 8.5	9.2 ± 2.1
Surgeon 5	23.1 ± 2.8	7.9 ± 2.1
All	23.9 ± 6.6	8.4 ± 0.5

Case 1: The first case covers a comparison of one special design with 4 sequential universal joints $4LU$ (e.g. [3]) to point out the influence of the joint limits $q_{lim,py}$ (Eq.19) and the geometric parameters. In Fig. 6, different alternatives in the design space, that is SUR over d_{IB}, are depicted as different symbols ×, □, ◯ and △. Black symbols belong to the mean Shaft Distance criterion whereas blue symbols indicate the standard deviation. Obviously, greater joint ranges θ_{lim} increase the number of successfully performed knots, see the design × with a joint range of $q_{lim,py} = \pm 22.5°$ and design ◯ with a joint range of $q_{lim,py} = \pm 35°$. A greater linear transmission ratio i_{kin} increases the SUR-measure further, see design △ with $i_{kin} = 1.5$. Therefore, an instrument designer is able to find a trade off between greater joint range and a greater transmission ratio, in case he wants achieve certain values for SUR and d_{IB}. Moreover, a smaller link length l_{link} decrease the mean distance d_{IB} and its standard deviation as well as slightly increasing the SUR-criterion, see designs ◯, $l_{link} = 10$ mm and □, $l_{link} = 5$ mm. The presented results are summarized in Tab. V.

TABLE V
Case 1: Comparison of alternatives towards a 4link design with universal joints $4LU$

design	$q_{lim,py}\,[°]$	$SUR\,[\%]$	$d_{IB} \pm std\,[mm]$
$4LU_{l10,i1,l}$	±22.5	27.8	15.2 ± 4.9
$4LU_{l10,i1}$	±35	49.1	15.2 ± 4.8
$4LU_{l5,i1}$	±35	51.2	8.2 ± 2.5
$4LU_{l10,i1.2}$	±35	59.1	13.1 ± 4.0

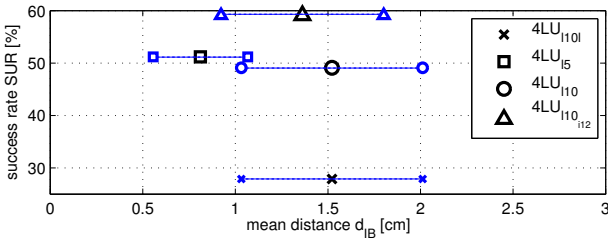

Fig. 6. Design space for alternatives towards a 4link design with universal joints $4LU$. $\times$-design: $l_{link} = 10, i_{kin} = 1.0, \theta_{lim} = 22.5°$ (l = low), $\square$-design: $l_{link} = 5, i_{kin} = 1.0, \theta_{lim} = 35.0°$, $\bigcirc$-design: $l_{link} = 10, i_{kin} = 1.0, \theta_{lim} = 35.0°$, $\triangle$-design: $l_{link} = 10, i_{kin} = 1.2, \theta_{lim} = 35.0°$

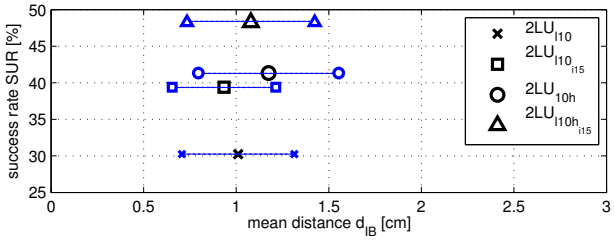

Fig. 7. Design space for alternatives towards a 2 link design with universal joints $2LU$. $\times$-design: $l_{link} = 10, i_{kin} = 1.0, \theta_{lim} = 45.0°$, $\square$-design: $l_{link} = 10, i_{kin} = 1.5, \theta_{lim} = 45.0°$, $\bigcirc$-design: $l_{link} = 10, i_{kin} = 1.0, \theta_{lim} = 60.0°$ (h = high), $\triangle$-design: $l_{link} = 10, i_{kin} = 1.5, \theta_{lim} = 60.0°$ (h = high)

Case 2: For this case, a preferred instrument design is previously chosen, here a 2link design with universal joints with a fixed link length of $l_{link} = 10$ mm is demanded. The initial joint limits are $q_{lim,py} = 45°$. The defined design goals are a maximum of $d_{IB} = 1.5$ cm (confined space in minimally invasive intervention) and the successful performance of the knot in at least $N_c = 300$ feasible poses yielding a SUR-value of at least 41%.
Starting with the design $\times$ in Fig. 7, the distance criterion is fulfilled whereas the achieved $SUR = 30.2\%$ is too low. In order to get an increase, the designer can enlarge the joint range to $q_{lim,py} = \pm 59°$ (design $\bigcirc$) or the linear transmission ratio to $i_{kin} = 1.5$ (design $\square$). The first alternative yields the requested increase in the SUR but also an increase in the distance criterion d_{IB} over the set threshold. The greater transmission ratio (design $\square$) also stays below the requested value in d_{IB} and yields an increase in SUR-value to 39.4% which is significantly higher but still below the requested value of $SUR = 41\%$. Design $\triangle$ combines the higher joint limit and the higher gear ratio to fulfill both criteria. Now, the joint limit could even be decreased again, since $SUR = 48.3\%$ is by far higher as the requested. The presented results are summarized in Tab. VI.

Case 3: Starting point for this third case is a well known design and the corresponding SUR and mean d_{IB} acquired in an evaluation with this method. The well known design here is the 2link design with 2 joints ($2\text{LPY}_{l5,i1}$) from [4] which is already applied in real minimally invasive interventions. The achieved performance is presented in Tab. VII, highlighted in grey. Design alternatives are a 4link and a 2link design with univeral joints and a link length of $l_{link} = 5$ mm ($4\text{LU}_{l5,i1}$, $2\text{LU}_{l5,i1}$) and a $l_{link} = 10$ mm ($2\text{LU}_{l10,i1}$). Furthermore, a 4link PYYP design [6] is considered, also with a link length of $l_{link} = 5$ mm ($4\text{LPYYP}_{l5,i1}$). The linear ratio is set to $i_{kin} = 1.0$. The goal within this case would be to find a set of design parameters for a instrument design that meets the performance of the well known instrument. After having maximum values for the distance criterion d_{IB} and the success rate SUR, a designer is able to select between the alternatives listed in Tab. VII. The proposed method would suggest the design $2\text{LU}_{l5,i1}$ with an increase in SUR and a decrease in d_{IB}.

TABLE VI

CASE 2: COMPARISON OF ALTERNATIVES TOWARDS A 2LINK DESIGN WITH UNIVERSAL JOINTS $2LU$

design	$q_{lim,py}\,[°]$	$SUR\,[\%]$	$d_{IB} \pm std\,[mm]$
$2\text{LU}_{l10,i1}$	± 45	30.2	10.0 ± 3.2
$2\text{LU}_{l5,i1}$	± 45	39.4	9.3 ± 2.7
$2\text{LU}_{l10,i1,h}$	± 59	41.3	11.8 ± 3.6
$2\text{LU}_{l10,i1.5,h}$	± 59	48.3	10.9 ± 3.1

Case 4: This last case highlights the possible application within the preoperative planning of a minimally invasive intervention. During the planning phase, the trocar locations are determined based on the location and orientation of the area of interest, approximated as a plane surface. Therefore, the created set of initial suture line orientations (Eq.11) can be reduced to a subset since only relevant suture lines from the set $\boldsymbol{W}_{SL}$ need to be considered. Relevant suture lines in this case are suture lines that match the planned orientation of the plane area. Suture lines varying in 360° are considered on this plane and therefore the relevant subset can be extracted. Considering a gentle approach, see Fig. 1 right bottom, with a horizontal orientation of the organ (plane area of interest). The angle between the shaft axis and the plane is approximated as 45°. Therefore suture lines for $\beta_i = 0°/60°$ are considered.
The same instrument alternatives are considered as in the prior case and the relevant data for the preoperative planning are listed in Tab. VIII. The comparison suggests to select either the design in row 3 ($2\text{LU}_{l5,i1}$) or the design in row 5 ($4\text{LPYYP}_{l5,i1}$) depending on the available space. With $N = 306$ poses considered in this planning phase, the $4\text{LPYYP}_{l5,i1}$ design would accomplish 244 poses which are 16 more than the design $2\text{lS}_{l5,i1}$ with 228, yielding the application of this design.

V. CONCLUSION

The paper in hand presented a new method to evaluate alternative instrument kinematics w.r.t. their ability to perform a surgical task. Sec. II classified available instrument designs from literature and presented a review of equivalent evaluation methods. In Sec. III, two criteria were developed. The *Shaft Distance* criterion d_{IB} which accounts for the confined space during a minimally invasive intervention and the

TABLE VII

CASE 3: COMPARISON OF DIFFERENT INSTRUMENT DESIGN ALTERNATIVES

design	$q_{lim,py}\,[^\circ]$	$SUR\,[\%]$	$d_{IB} \pm std\,[mm]$
$2\text{LPY}_{l5,i1}$	± 89	30.5	4.9 ± 1.7
$4\text{LU}_{l5,i1}$	± 22.5	31.8	8.1 ± 1.8
$2\text{LU}_{l5,i1}$	± 45	31.9	5.0 ± 0.8
$2\text{LU}_{l10,i1}$	± 45	30.2	9.7 ± 2.2
$4\text{LPYYP}_{l5,i1}$	± 45	32.6	8.4 ± 2.1

TABLE VIII

CASE 4: COMPARISON OF DIFFERENT INSTRUMENT DESIGN ALTERNATIVES WITHIN EXEMPLARY PREOPERATIVE PLANNING

design	$q_{lim,py}\,[^\circ]$	$SUR\,[\%]$	$d_{IB} \pm std\,[mm]$
$2\text{LPY}_{l5,i1}$	± 89	76.1	0.5 ± 0.2
$4\text{LU}_{l5,i1}$	± 22.5	79.2	0.8 ± 0.2
$2\text{LU}_{l5,i1}$	± 45	79.6	0.5 ± 0.1
$2\text{LU}_{l10,i1}$	± 45	75.4	0.97 ± 0.3
$4\text{LPYYP}_{l5,i1}$	± 45	81.3	0.85 ± 0.2

Success Rate SUR which accounts for the ability to execute the desired task. The evaluation is based on task specific trajectories which are recorded from expert surgeons in an open surgery test bed. Experimental overhead is minimized since reference frames were varied in software to account for arbitrary orientations of e.g. the suture line. In contrast to the proposed methods from the literature, it is independent from the setup, i.e. the relative position and orientation of the area of interest w.r.t. the trocar location. These trajectories can range from e.g. a single needle insertion to a series of knots tied along a suture line. Remarks on the applied forward and inverse kinematics and on the implementation of the method can also be found in Sec. III. Four different application cases in Sec. IV illustrate possible use cases of the method.

A useful feature of the method is the ability to apply different task trajectories. In the future, we want to apply other standardized task like retracing pegboard patterns or cutting predefined patterns [21] as well as e.g. a single needle insertion. Furthermore, we want to focus on finding unified benchmarks that represent trajectories recored from several different surgeons. Since redundant instrument kinematics are omitted in the presented method, we will also focus on extending it towards this case.

REFERENCES

[1] U. Seibold, B. Kübler, and G. Hirzinger, "Prototype of instrument for minimally invasive surgery with 6-axis force sensing capability," IEEE International Conference on Robotics and Automation (2005): pp. 496-501.

[2] K. Harada, "Micro manipulators for intrauterine fetal surgery in an open MRI," IEEE International Conference on Robotics and Automation (2005): pp. 502-507.

[3] P. Berkelman and J. Ma, "A compact modular teleoperated robotic system for laparoscopic surgery," The International Journal of Robotics Research 28(9) (2009): pp. 1198-1215.

[4] A.J. Madhani and J. K. Salisbury, "Articulated surgical instrument for performing minimally invasive surgery with enhanced dexterity and sensitivity," U.S. Patent No. 5,792,135. 11 Aug. 1998.

[5] G. Darbemamieh, S. Najarian, S. Mosafer, "Design and analysis of a mechanism for enhanced flexibility in minimally invasive surgical instruments," Cairo International Biomedical Engineering Conference (2010): pp. 90-93.

[6] T. G. Cooper, D.T. Wallace, S. Chang, S. C. Anderson, S. Manzo "Surgical tool having positively positionable tendon-actuated multi-disk wrist joint," U.S. Patent No. 6,817,974. 16 Nov. 2004.

[7] N. Simaan, "Snake-like units using flexible backbones and actuation redundancy for enhanced miniaturization," IEEE Intenational Conference on Robotics and Automation (2005): pp. 3012-3017.

[8] G. Kunad, J. Müglitz, P. Dautzenberg, B.Neisisus, R. Trapp , Getriebebewegliche Instrumente fr die Minimal Invasive Chrirurgie, VDI Berichte, vol. 1111, pp. 333-349, 1994

[9] B. Roth, Performance evaluation of manipulators from a kinematic viewpoint. NBS Special Publication 459 (1976): 39-62.

[10] A. Kumar, and K. J. Waldron, The workspaces of a mechanical manipulator, American Society of Mechanical Engineers, Design Engineering Technical Conference, Beverly Hills, Calif. 1980.

[11] R. Konietschke, Planning of Workplaces with Multiple Kinematically Redundant Robots, dissertation, Institute for Real Time Computer Systems, TU Muenchen, Germany, 2007.

[12] K. Ankur, N. Simaan, and R. H. Taylor, "Suturing in confined spaces: constrained motion control of a hybrid 8-DoF robot," IEEE International Conference on Advanced Robotics (2005): pp. 452-459.

[13] J. Ding, K. Xu, R. Goldman, P. Allen, D. Fowler and N. Simaan, "Design, Simulation and Evaluation of kinematic alternatives for insertable robotic effectors platforms in single port access surgery," IEEE International Conference on Robotics and Automation (2010): pp. 1053-1058.

[14] A. Faraz, and P. Shahram, "Synthesis and workspace study of endoscopic extenders with flexible stem," Transactions of the ASME-R-Journal of Mechanical Design 119.3 (1997): 412-413.

[15] J. Craig, "Introduction to Robotics: Mechanics and Control," 3rd ed., 3. Pearson Prenctice Hall, 2005.

[16] M. Cenk Cavusoglu, I. Villanueva, and F. "Tendick, Workspace analysis of robotic manipulators for a teleoperated suturing task," IEEE International Conference on Intelligent Robots and Systems (2001): pp. 2234-2239.

[17] T. Yoshikawa, "Manipulability of robotic mechanisms," The International Journal of Robotics Research 4.2 (1985): 3-9.

[18] A.H. Zahraee, J.K. Paik, J. Szewczyk, G. Morel,"Toward the development of a hand-held surgical robot for laparoscopy," IEEE/ASME Transactions on Mechatronics, 15(6), (2010) 853-861.

[19] C. A. Klein, and B. E. Blaho, "Dexterity measures for the design and control of kinematically redundant manipulators," The International Journal of Robotics Research 6.2 (1987): 72-83.

[20] K.A. Guru, M.R. Sheikh, S.J. Raza, A.P. Stegemann, J. Nyquist, Novel Knot tying technique for robot assisted surgery, The Canadian Journal of Urology 19(4) (2012): 6401-6403.

[21] A.M. Derossis, G.M. Fried, M. Abrahamowicz, H.H. Sigman, J.S. Barkun, J.L. Meakins, Development of a Model for Training and Evaluation of Laparoscopic Skills, The American Journal of Surgery, 175 (1998): 482-487.

[22] R.R. Gopaldas and R.M. Reul, Intracorporeal Knot-Tying for the Thoracoscopic Surgeon. A Novel and Simplified Technique, Texas Heart Institute Journal 37(4) (2010): 435-438

[23] P.J. Lopez, J. Veness, A. Wojcik, J. Curry, How Reliable Is Intracorporeal Laparoscopic Knot Tying, Journal of Laparoendoscopic & Advanced Surgical Techniques, 16(4) (2006): 428-433.

[24] A. Wimmer, B. Deutschmann, B. Kübler, C. Rink, and G. Hirzinger, "Spine Kinematic with Constrained Guidance for Minimally Invasive Robotic Surgery," IEEE International Conference of Robotics and Automation (2013): pp. 5433-5440.

[25] M. Lohmann, R. Konietschke, A. Hellings, C. Borst and G. Hirzinger, "A workspace analysis method to support intraoperative trocar placement in minimally invasive robotic surgery," Proceedings of the German association of robotic surgery 2012.